Fuel xxx (xxxx) xxx

Contents lists available at ScienceDirect

Fuel

journal homepage: www.elsevier.com/locate/fuel

Full Length Article

Prediction of the flame kernel growth rate in spark ignition engine fueled with natural gas, hydrogen and mixtures

Blanca Giménez [a,*], Andrés Melgar [a], Alfonso Horrillo [b], Pedro Gabana [a]

[a] Department of Energy and Fluid Mechanics Engineering, University of Valladolid, Paseo del Cauce 59, E-47011 Valladolid, Spain
[b] CIDAUT Foundation, Plaza Vicente Aleixandre Campos 2, Parque Tecnológico, E-47151 Boecillo-Valladolid, Spain

ARTICLE INFO

Keywords:
Flame kernel growth
Natural gas-hydrogen mixture
Quasi-dimensional combustion model
Homogeneous combustion
Laminar to turbulent combustion transition
Pressure records diagnostic

ABSTRACT

The knowledge of combustion duration is a key tool in the development of engines, specially nowadays for engines adapted to new fuels with low C/H ratio such as natural gas and hydrogen. This work is aimed to develop a correlation that predicts the duration of the first phase of combustion until the process becomes turbulent in a SI engine. The flame kernel radius when this transition occurs, R_{tr}, is the study variable.

To determine this variable from the experimental pressure records, a flame kernel growth predictive model is used. The predictive model is adjusted to the experimental data, determining the most appropriate R_{tr} value.

The pressure records of 500 consecutive cycles of 48 test points have been processed. The averaged values of R_{tr} of each test point have been correlated with the characteristic parameters of the process: turbulence and properties of the fuel–air mixtures. Finally, R_{tr} and integral length scale ratio is correlated with Damköhler number.

A wide range of operating conditions have been studied, reaching the novel conclusion that it is possible to analyze the kernel growth phenomenon from a spatial point of view rather than from a temporal point of view, as had been studied in many previous works.

The developed correlation can be used in combustion predictive modeling to support SI engine design. Other practical conclusion from the work, that can be used in SI engine development, is that decreasing the integral length scale reduces the time of the first phase of combustion.

1. Introduction

In spark-ignition engines (SIE), the combustion process begins under thermodynamic and turbulence levels that depend on the engine operating conditions. These conditions affect the evolution of the combustion process in the first stages.

This first stage of combustion has certain characteristics that differentiate it from the rest of the combustion process. One of the most critical is that the area of the flame front is small, which justifies the low values of heat release rate, even though the combustion speed is turbulent. This causes that the angular interval from start of ignition (SOI) until 10 % of the mixture is burnt (CA010) is similar to the time it takes to burn from 10 % to 90 % of the mixture (CA1090) for stoichiometric fuel–air equivalence ratio and it can be higher in case of poor fuel–air equivalence ratio [1,2].

The analysis of the combustion onset, which covers approximately half of the total combustion duration, arouses great interest and can provide ideas for improving the SIE performance, consequently it is the aim of several research works.

In the model developed by Herweg et al. [3] it is pointed out that at the beginning of the process the combustion speed is close to laminar, however, as the flame front size increases, the combustion speed is affected by turbulence. Ayala et al. [1] propose a model for the flame kernel development based on the concept of a laminar combustion process onset that evolves into a turbulent one. These authors propose a model dependent on the Taylor microscale size, since they consider that the interaction zone between these eddies is where turbulent combustion takes place.

These two previous works propose models for the combustion speed growth similar to a first-order system response to a step function, $1-e^{-kt}$, so that at first it grows very quickly and then tends asymptotically to the final value.

The first stage of combustion is divided in [3,4]: ignition and flame initiation; flame kernel growth at laminar flame speed, transition from

* Corresponding author.
E-mail addresses: blagim@eii.uva.es (B. Giménez), andmel@eii.uva.es (A. Melgar), alfhor@cidaut.es (A. Horrillo), pedro.gabana@uva.es (P. Gabana).

https://doi.org/10.1016/j.fuel.2022.126908
Received 9 September 2022; Received in revised form 21 November 2022; Accepted 23 November 2022

laminar to turbulent speed propagation and fully developed flame propagation. According to these authors, almost all the factors that affect the first affect the second, so it is usual to distinguish only between initial combustion (which includes the first two mentioned above) and main combustion. Part of the work presented in this paper consists of modeling this first phase with a novel approach.

Combustion in a SIE starts with a volume of unburned products which size is the spark plug gap, typically 1 mm. In the middle of this volume, an electric spark ionizes and converts the mass of unburned products in plasma at a temperature of several thousand degrees. This initial kernel expands due to the high temperature and later a flame front separates the burned mass from the unburned mass. Due to the high temperature of the burned mass, the flame front progresses at a speed one order of magnitude greater than the corresponding to a laminar process. This speed decreases rapidly to values corresponding to a laminar process. Experimental results confirming this approach have been obtained in both constant volume combustion bombs [5–7] and in internal combustion engines [2,8,9].

In this way, Eisazadeh-Far et al. [10] present some experimental images of the flame kernel growth taken in a flammable medium and in air. The experiments were done in a constant volume bomb during the spark ignition phase. These authors propose a model of the development of this first phase with and without combustion. The study is done in a quiescent environment.

A similar work, but with air movement is done by R. Maly [11], a model to analyze the flammability limits of different mixtures is also presented. In a later work, Herweg et al. [3] carried out an engine study visualizing the evolution of the flame front during the first stage of combustion. They also propose a thermodynamic model of the flame kernel evolution, taking into account the energy applied by the ignition spark. These works show that the temperature reached in the SOI leads to a very high combustion speed and, additionally, as the mass is small with respect to its growth rate, the initial spark energy is diluted, causing a fast decrease in the burned zone temperature. The temperature is stabilized at a value close to the adiabatic flame temperature. From this point the advance of the flame front occurs at a combustion speed close to the laminar.

The models proposed in [3,8,10,12] agree that the energy released in the spark discharge that is not dissipated to the electrodes, is used to increase the internal energy of the burned mass. Pischinger et al. [13] state that the laminar combustion speed after the spark discharge is multiplied by a factor proportional to the ratio of the temperature difference of the burned mass and the theoretical temperature at which the flame quenching would occur, $T_b - T_q$, versus the temperature difference that there would be in a laminar combustion process without an external heat source T_{ad} and T_q. In the model presented in this work, this approach is taken into account to consider the energy provided by the spark.

The phases following the first stage of combustion take place when the kernel reaches a certain size. At that moment a transition begins, and the combustion speed grows until values corresponding to a turbulent process.

In the analysis of this transition, various experimental works have also been carried out, mainly visualization of the flame front in the first moments of combustion. On the one hand, there are works on combustion bombs such as [7,11,12] and on the other hand there are experimental works in transparent engines [14–17]. These last two, have quantified the transition measuring the growth of the burned mass volume.

Peterson et al. [15] and Zeng et al. [17] measure the air velocity inside the cylinder with a PIV system and conclude that the flow pattern in the vicinity of the spark plug at the moment of ignition can generate different patterns of flame kernel development.

Several authors have tried to model this process, either through thermodynamic modeling as in [1,3,8,11–13] or by CFD modeling as in [18–23]. Some of these authors [19,20,23] set in 1.5 mm the traveled space by the flame front when the transition takes place. Some works such as [19,20,22,23] propose a hyperbolic tangent function to model the combustion speed transition from laminar to turbulent. Keum et al. [22] fits the transition model with experimental data, and the transition fit is different depending on whether the simulation is RANS or LES.

At another level and with another philosophy, Pera et al. [24] simulate the first phases of the combustion in SIE conditions, using DNS. The simulations are carried out by modifying the initial size of the flame kernel, the structure of the turbulence (initial velocity field pattern), the turbulence intensity and the integral length scale (the two latter understood as global variables of turbulence). An estimation of the CCV is made by the variation of the heat release at the end of several simulations. The study, for stoichiometric and poor fuel–air equivalence ratio, concludes that for both cases, the initial size of the flame kernel and the structure of the turbulence are the most determining parameters in the CCV.

Other authors such as Salvi et al. [25] try to characterize experimentally the flame kernel development process. In this case it is done through the average flame front speed from the SOI until it reaches the periphery of the spark plug. The study has been done for several fuel–air equivalence ratios and several SOI points. They develop a correlation of the flame kernel growth rate depending on operating conditions such as the engine speed, pressure and fuel–air equivalence ratio.

Most of the works above are oriented to study the duration of the first phase of combustion until the process becomes turbulent, on the one hand by investigating through experimental work aimed to measure the duration of this time interval and, on the other hand by modeling the process and adjusting the model with information obtained from experiments. These works generally cover a small range of engine operating conditions. In many cases this is because of the problems involved in experimentation with optical access. Something similar occurs in the case of CFD modeling where computational requirements limit the simulations number.

In the development of an engine, it would be valuable to have estimations of the first stage combustion duration, for all operating conditions of the engine and fuels to be used. This estimation will allow to predict the engine behavior during the basic design phase.

The objective of this work aims to simplify the calculation of the duration of the first phase of combustion by means of a correlation covering a wide range of engine operating conditions using fuel blends, which is a novelty compared to previous work. For this purpose, engine pressure records under multiple operating conditions and different fuels have been analyzed.

With these data a combustion initiation model has been fitted using the flame front radius in which the combustion becomes turbulent, R_{tr}, as parameter. This radius has been correlated as a function of characteristic parameters at SOI. Therefore, the correlation can be used to improve the predictive ability of SIE combustion models: dimensional models (CFD) and quasi-dimensional models (thermodynamic combined with geometrical model).

In our previous work [26] pressure records in the combustion chamber are used as input to a two zone quasi-dimensional diagnostic model. The turbulent combustion speed is determined once the flame front is fully developed and advances at a combustion speed imposed by the turbulence levels in the combustion chamber. The diagnostic model uses the pressure derivative to determine the combustion speed. During the first phase of combustion, pressure recording noise does not allow to obtain a reliable pressure derivative value so it is not possible to obtain information about the combustion process from the pressure records in this phase.

In addition to the study of Giménez et al. [26], this work focuses on identifying the evolution of the combustion speed in the first stages of combustion, which was not considered in the previous work, where only a diagnostic model was used. For that, in this work, under certain hypothesis of combustion speed behavior in the first stages of combustion, a two-zone quasi-dimensional predictive model based on a spherical flame front centered on the spark plug is used for calculating the pressure at combustion beginning. The model uses a hyperbolic tangent function to simulate the combustion speed transition from laminar to turbulent. The flame front radius where this transition occurs, R_{tr}, is adjusted so that the calculated pressure at the end of the first phase of

combustion agrees with experimental pressure value in the same point. Thus, it is not necessary to use the pressure derivative in this phase.

The predictive model considers that the laminar burning speed before the transition is affected by the high temperatures of the unburned products due to the energy freed by the spark plug.

Different mixtures of natural gas and hydrogen are used in experiments with different fuel–air equivalence ratios and engine speeds. For each of the 48 test points, the position of the transition R_{tr} has been adjusted in 500 consecutive cycles. The averaged results of each test point have been related to other characteristic variables of the combustion process.

A correlation of the position of the transition, R_{tr}, has been obtained. The correlation can be used in predictive models to estimate this position as a function of different operating variables and finally predict the duration of this first stage of combustion.

The rest of the paper is structured as follows: In section 2 the methodology of pressure data processing and the equations used in the predictive model are presented; In section 3 the experimental test points and their position on the Borghi-Peters diagram are presented; In section 4 the average results are analyzed and correlated; Finally, in section 5 the more important conclusions and the results utilization are discussed.

2. Methodology

2.1. Processing of pressure records.

The pressure records have been processed following the next steps:

1. Filtering of pressure records using a polynomial regression. For pressure determination in the interval between two experimental data (0.6 crankshaft degrees), the 10 data before and the 10 after the interval have been used to calculate the 5th order polynomial with the lowest mean square error, as if using a Savitzky-Golay filter [27], but with the result of a continuous function that allows to calculate the value of the pressure and its derivative, dp/dt, at any CA. At the beginning of combustion, the average of the difference between the experimental data and the filtered data for all cycles is lower if polynomials of order 5 are used instead of 4 order polynomials used in Giménez et al. [26]. A higher polynomial order means not filtering enough and obtaining excessive noise in the dp/dt value.
2. Determination of pressure and angle offsets, compression ratio and heat transfer coefficient. For this, a methodology based on genetic algorithms is used, as stated by Reyes et al. [28].
3. Processing of the filtered pressure data with a diagnostic thermodynamic model. The diagnostic model allows calculating the burned mass rate, dm_b/dt, from dp/dt obtained processing experimental pressure data. During first stages of combustion, this model is not accurate enough to be used for S_d calculus in next step.
4. Processing of the resulting data with a geometric model to calculate the turbulent combustion velocity, S_d. A hemispherical flame front centered at the spark plug position is assumed. The geometric model for calculating the front area is described by Giménez et al. [26]. S_d results are only valid when the combustion process is fully developed.
5. At the combustion beginning, it is not possible to calculate the combustion speed S_d using the diagnostic model due to low accuracy of the pressure data. The behavior of the combustion speed in this first stage should make the pressure develops according to the experimental data. In this work it is assumed that during the first stages the combustion speed behavior is a transition from laminar to turbulent [1,3,14–17] and this occurs for a given flame kernel size [19,20,22,23]. Thus, it is possible to calculate dm_b/dt and use it in a predictive model to calculate dp/dt at early stages of combustion.
6. For each cycle the flame front radius in which the transition of the combustion speed from laminar to turbulent occurs, R_{tr}. is adjusted so that the calculated pressure evolution during first stages of combustion agrees with experimental pressure data.

2.2. Predictive and diagnostic models description.

This section describes how to calculate the combustion speed S_d from the pressure in the combustion chamber using a diagnostic model composed of a thermodynamic model (Eq.(1), (2), (3), (4)) and later a geometric model (Eq. (5)). It is also described how to rearrange the equations of the model to calculate the pressure in the combustion chamber from the combustion speed S_p with a predictive model that employs a geometrical model Eq. (6) and later a thermodynamic model Eq. (7), (2), (3), (4).

The two zones diagnostic model used is the same as that presented by Giménez et al. [26] and [29]. The thermodynamic model is based on four differential equations: two for mass and specific energy of the unburned zone, dm_u/dt and du_u/dt, and other two for the same variables in the burned zone, dm_b/dt and du_b/dt. The model input is the experimental pressure record, from which dp/dt is calculated and substituted into equations (1), (2), (3) and (4).

$$\frac{dm_b}{dt}=\frac{\frac{dp}{dt}\left(m_u v_u \frac{\gamma_b^*}{\gamma_u}+m_b\left(v_b+\left(\gamma_b^*-1\right)\frac{\partial u_b}{\partial p}\right)\right)-\left(\frac{\gamma_u-1}{\gamma_u}\gamma_b^*\dot{Q}_u+\left(\gamma_b^*-1\right)\dot{Q}_b\right)+p\gamma_b^*\left(\frac{dV(\alpha)}{dt}+v_u\dot{m}_{bb}\right)}{\gamma_b^*(u_u-u_b)+(h_u-h_b)} \tag{1}$$

$$\frac{dm_u}{dt}=-\frac{dm_b}{dt}-\dot{m}_{bb} \tag{2}$$

$$\frac{du_u}{dt}=\left(\frac{dp}{dt}v_u+\dot{q}_u\right)\frac{1}{\gamma_u} \tag{3}$$

$$\frac{du_b}{dt}=\begin{cases}\left(\frac{dp}{dt}\left(v_u+\left(\gamma_b^*-1\right)\frac{\partial u_b}{\partial p}\right)+\dot{q}_u\right)\frac{1}{\gamma_b^*} & m_b\cong 0\\ \frac{dm_b}{dt}\frac{(u_u-u_b)}{m_b}-\frac{dp}{dt}\frac{v_u m_u}{\gamma_u m_b}+\frac{1}{m_b}\left(\frac{\gamma_u-1}{\gamma_u}\dot{Q}_u+\dot{Q}_b\right)-\frac{p}{m_b}\left(\frac{dV(\alpha)}{dt}+v_u\dot{m}_{bb}\right) & m_b>0\end{cases} \tag{4}$$

$$c_{vb}^*=c_{vb}+\sum_{i=1}^{i=Z_b}\frac{\partial Y_{bi}}{\partial T}u_i(T_b)\gamma_b^*=\frac{c_{vb}^*+R_b}{c_{vb}^*}\frac{\partial u_b}{\partial p}=\sum_{i=1}^{i=Z_b}\frac{\partial Y_{bi}}{\partial p}u_i(T_b)$$

Once the thermodynamic problem has been solved, the flame front area can be calculated using the geometric model and finally the diagnostic combustion speed S_d.

$$S_d = \frac{\frac{dm_b}{dt}}{A_f \rho_u} \tag{5}$$

These equations can be rearranged to be used in a predictive model aimed to calculate the pressure in the combustion chamber from the combustion speed. For this purpose, Eq. (5) from the diagnostic geometric model is rewritten to calculate the burned mass rate dm_b/dt by means of the predictive combustion speed S_p (which will be covered in section 2.3):

$$\frac{dm_b}{dt} = S_p A_f \rho_u \tag{6}$$

Knowing dm_b/dt it is possible to reformulate Eqs. (1), (2), (3), (4) to have a predictive thermodynamic model with the variables dm_u/dt, du_u/dt, du_b/dt and dp/dt. In the predictive model differential equations system, the new unknown is dp/dt instead of dm_b/dt, resulting Eq. (1) as follows:

$$\frac{dp}{dt} = \frac{\frac{dm_b}{dt}\left(\gamma_b^*(u_u - u_b) + (h_u - h_b)\right) + \left(\frac{\gamma_u - 1}{\gamma_u}\gamma_b^*\dot{Q}_u + \left(\gamma_b^* - 1\right)\dot{Q}_b\right) + p\gamma_b^*\left(\frac{dV(\alpha)}{dt} + v_u\dot{m}_{bb}\right)}{m_u v_u \frac{\gamma_b^*}{\gamma_u} + m_b\left(v_b + \left(\gamma_b^* - 1\right)\frac{\partial u_b}{\partial p}\right)} \tag{7}$$

Eq. (7) allows calculating the pressure in the combustion chamber from the burned mass rate. Knowing dp/dt, Eqs. (2), (3), (4) can be used to calculate the derivatives of the remaining variables. Therefore, the new system of four equations consists in Eqs. (7), (2), (3), (4).

2.3. Determination of the predictive combustion speed S_p at combustion beginning

For the determination of S_p, a function depending on flame kernel radius R is used. It is assumed that immediately after the SOI, the combustion speed is high due to the thermal level of the burned zone achieved by the energy provided by the spark plug. Afterwards, it is reduced to values close to the laminar combustion speed S_l due to the burned mass cooling, and subsequently, S_p increases due to a transition to turbulent combustion velocity. When the flame front radius is R_{d_ini}, S_p value corresponds to the calculated with the diagnostic model one S_{d_ini}. The value of the flame front radius at the instant in which the transition from laminar to turbulent combustion occurs, R_{tr}, must be adjusted so that the calculated pressure is the same as the experimental pressure.

At SOI, the burned mass is equal to the unburned mass that occupies a volume equal to a sphere located between the spark plug electrodes (1 mm). The internal energy (which includes the formation internal energy) of that initial mass increases with the energy freed by the spark. This means that the burned zone temperature at the initial instant is much higher than the adiabatic flame temperature T_{ad} [10]. This high temperature of the burned mass is reflected in the fact that the combustion speed in these first moments is significantly higher than the laminar one, since the heat flux from the burned zone to the unburned zone is much higher than what would occur in a normal combustion process.

To consider this effect, the laminar combustion speed S_l, calculated with the correlation of Bougrine et al. [30], is modified by multiplying it by the ratio of the two zones temperature difference $T_b - T_u$ and the difference that there would be in a combustion process without an external heat source $T_{ad} - T_u$, in a similar way to Pischinger et al. [13] but using the unburned temperature instead of the quenching temperature.

$$S_{l\_mod} = S_l \frac{T_b - T_u}{T_{ad} - T_u} \tag{8}$$

S_{l_mod} has an asymptotic trend toward S_l as the temperature of the burned mass approaches the adiabatic temperature T_{ad}. As shown in Fig. 1, this effect is rapidly attenuated as the burned mass increases, since the energy provided by the spark is distributed with more mass, becoming very little influential on the burned mass temperature.

This initial speed evolves towards the turbulent combustion speed when the flame front radius takes the transition value R_{tr}. This transition is modeled as in [19,20,22,23] with a hyperbolic tangent dependent on

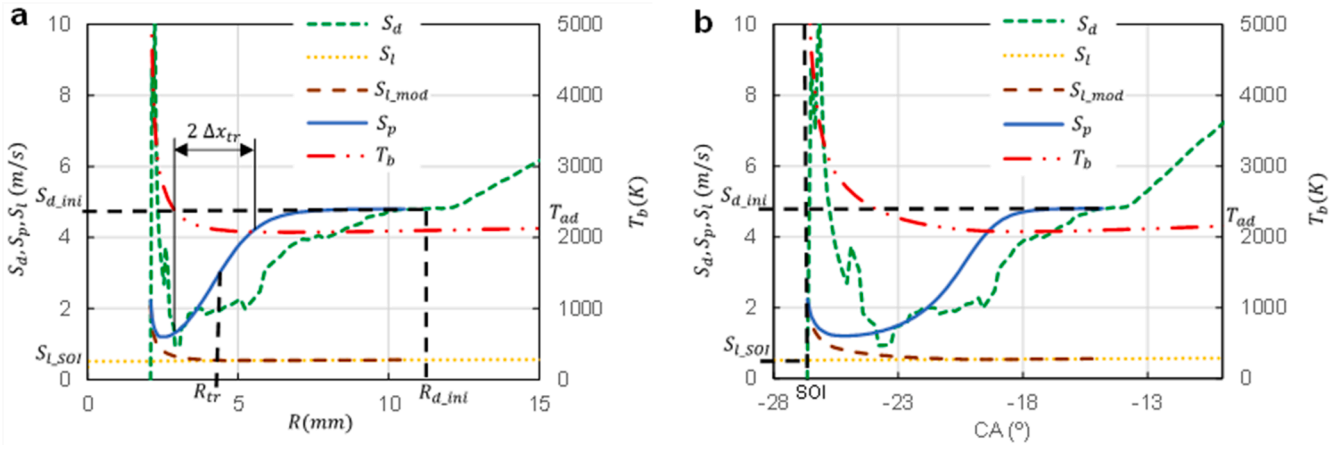

Fig. 1. Laminar combustion speed S_l, combustion speed used in the predictive model S_p, and turbulent combustion speed calculated with the diagnostic model S_d, and burned mass temperature T_b, (a) versus the flame front radius, (b) versus the crank angle degree.R_{tr} = 4.15 mmΔx_{tr} = 1.5 mm. Test NGH2 50 %, 1750 rpm, cycle 250.

the flame front radius R. Therefore, the combustion speed input to the predictive model S_p during the flame Kernel development interval is given by Eq. (9).

$$S_p = S_{l\_mod} + (S_{d\_ini} - S_{l\_mod})\frac{1}{2}\left[1 + tanh\left(\frac{R - R_{tr}}{\Delta x_{tr}}\right)\right] \quad (9)$$

The origin of the hyperbolic tangent function is the position at which the flame front radius R has a value equal to transition radius R_{tr}. Around this point, the combustion speed changes from the modified laminar burning speed, S_{l_mod}, to the turbulent combustion speed S_{d_ini}. The spatial interval in which the change occurs is fixed with Δx_{tr} whose value affects the slope at the origin of the hyperbolic tangent function, in short, the abruptness of the transition.

It has been decided to set $\Delta x_{tr} = 1.5mm$, the same value used in [19,20,23]. The radius for which the results of the diagnostic model are considered reliable R_{d_ini} has been set in 11 mm where the mass burned fraction depends on the test point, varying between 2 % and 3.6 %.

Fig. 1 shows the diagnostic S_d, predictive S_p and laminar S_l combustion speeds and the temperature of the burned mass T_b for a specific cycle (GNH2 50 %, 1750 rpm, cycle 250). The results are presented as a function of the flame front radius (a) and the crank angle degrees (b).

The combustion speed obtained with the diagnostic model S_d takes very different values when the flame front radius is small. The combustion speed used in the predictive model S_p, at the first phase of combustion, takes values higher than the laminar combustion speed S_l due to the high temperature of the burned products. S_p tends asymptotically to laminar speed as the burned mass temperature approaches the adiabatic flame temperature. The combustion speed of the predictive model S_p is equal to the combustion speed calculated with the diagnostic model S_{d_ini} at the flame front radius R_{d_ini}.

In Fig. 1(a) it is observed that there are no values for flame front radii lower than an initial value. This value corresponds to the radius of a hemisphere with the same volume that burned mass has at SOI. The hemispherical shape is due to the fact that the engine head is flat, and the ignition point is in the plane of the engine head. As has been said, the initial burned mass corresponds to the mass of unburned products contained in a sphere of diameter 1 mm (spark plug electrodes separation).

2.4. Iterative method for R_{tr} determination

The expression for dm_b/dt in Eq. (1) depends on dp/dt. During the first stage of combustion, the difference between the pressure values of the engine with combustion and without combustion is of the same order as the noise associated with the experimental record. Therefore, the diagnostic model is not valid to determine dm_b/dt in these first instants. Consequently, the combustion speed S_d cannot be calculated in an accurate way.

Since it is impossible to know the evolution of the combustion speed in the early instants, in this work we propose to use the model presented in section 2.3 to characterize the development of the flame kernel with a single spatial estimator R_{tr}. At this position of the flame front is where the transition from laminar combustion (calculated from the conditions in the combustion chamber with the Bougrine et al. [30] equation) to turbulent combustion takes place.

The predictive model differential equations are integrated into an angular interval that begins at SOI and ends in the angle where the flame front radius calculated with de diagnostic model reaches the value R_{d_ini} (in graphical abstract $CA(SOI)$ and $CA(R_{d\_ini})$). At this instant, it is considered that the burned mass m_b and the combustion speed S_{d_ini}, calculated with the geometric-diagnostic model has sufficient precision.

The amount of mass burned at the end of the angular interval depends on the value of R_{tr}. Therefore, for each cycle of each test point, the value of R_{tr} has been determined so that the mass burned calculated with the predictive model (using R_{tr}) at the end of the angular interval ($CA(R_{d\_ini})$) is the same as that calculated with the diagnostic model. If this occurs, the pressure calculated with the predictive model will coincide with the experimental one (used by the diagnostic model), and the radius of the flame front at the end of the interval will coincide with R_{d_ini}.

To determine the R_{tr} value that meets the conditions stated in the previous paragraph, the predictive model is run iteratively in the angular interval considered and a bisection method is used with the following initial values: the value of the radius of the flame front after SOI and R_{d_ini}. The graphical abstract shows a flow chart of the iterative process for R_{tr} calculation.

3. Experimental setup

The experimental data are the same as those used by Giménez et al. [26], the engine has a compression ratio of 11.15:1 with a stroke of 75 mm and a bore of 80 mm. All the information about the installation can be found in [26].

The test planning consists of 48 test points and is the same as in [26], with the difference that 500 cycles have been processed at each operating point.

Different fuel–air equivalence ratios have been chosen for the test points with NG (0.7, 0.8, 0.9 and 1.0), with H2 (0.4, 0.45, 0.5, 0.56, 0.6, 0.65, 0.7), and with NGH2 mixtures with percentages of H2 0 %, 25 %, 50 %, 75 % and 100 % (0.697, 0.686, 0.666, 0.633 and 0.536 respectively). The fuel–air equivalence ratios of the NGH2 mixtures have been chosen to have the same adiabatic flame temperature starting from the same initial conditions of pressure and temperature existing at top dead center in motored engine. For each of the 16 mixtures, experiments have been carried out with three engine speeds: 1000, 1750 and 2500 rpm (piston lineal mean speed 2.5, 4.4 and 6.25 m/s and turbulence levels at SOI u'=2, 3.25 and 4.4 m/s). SOI is chosen such that the maximum pressure is reached 10 CA degrees after top dead center.

The trapped mole number is the same in all test points (6000 μmol). This implies IMEP levels that are little dependent on engine speed and variable with the fuel/air equivalence ratio between 3 and 4 bar in NG and between 2.1 and 3.2 bar in H2. The maximum pressures achieved range from 23 to 30 bar in NG and from 20 to 31 bar in H2.

Fig. 2 shows the positions of all the test points at SOI on the Borghi-Peters diagram [31,32]. Only in GN 1750 rpm, ϕ=0.7 and GN2500 rpm, ϕ=0.7 and ϕ=0.8 test points the Kolmogorov scale is slightly lower than the thickness of the laminar flame front. Therefore, it can be considered that the combustion at the beginning is developed in the region of corrugated and wrinkled flamelets.

Fig. 3 shows the density ratio at SOI for all test points. It can be seen that the density ratio, σ, of NG is higher than the density ratio of H2 due to the mole number reduction in the hydrogen combustion process. The fuel air equivalence ratio increases the density ratio mainly due to a higher combustion temperature.

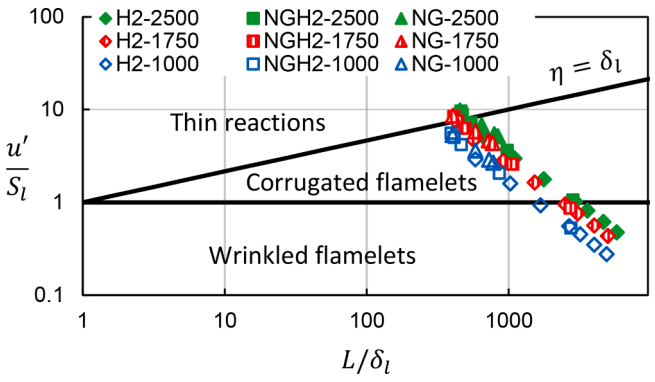

Fig. 2. Combustion regimes of the different test points at SOI.

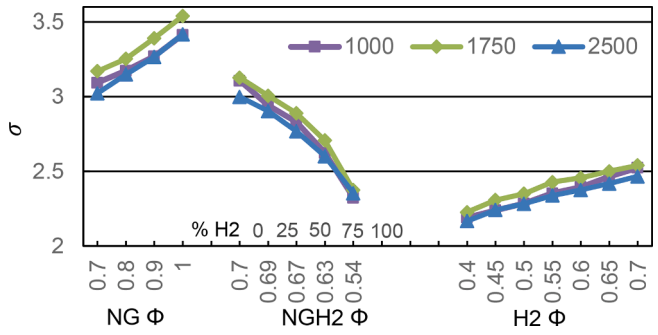

Fig. 3. Density ratio σ at SOI for each test point. 1000, 1750 and 2500 rpm.

4. Results

4.1. Mean results from experiments

Fig. 4 presents the average transition radius R_{tr} of 500 cycles for each of the 48 test points. A first conclusion is that the size of the flame front when the transition occurs is of the same order of magnitude of the distance from piston to engine head, which corresponds to the size of the integral scale of the turbulence L used in this work.

In the case of H2, there is no appreciable influence of the engine speed, however, in the case of NG and NG-rich mixtures, for the case of 1000 rpm, R_{tr} is slightly higher. This suggests that the value of the transition radius R_{tr} has a little dependence on the intensity of the turbulence in the combustion chamber confirming the hypothesis that the combustion speed is laminar at early stages of flame kernel growth [3]. There is a much greater dependence on fuel–air equivalence ratio in hydrogen than in natural gas. However, in the case of mixtures and NG, the trend is not clear and in any case is not as significant as in H2.

It could be concluded from these results that the variable that most affects R_{tr} is the laminar combustion speed S_l, especially when its value is high, which is the case of high fuel–air equivalence ratios of H2.

A characteristic transition time τ_{tr} is defined according to Eq. (10) corresponding to the time it would take for the flame front to reach R_{tr} at the laminar combustion speed at SOI, S_{l_SOI}:

$$\tau_{tr} = \frac{R_{tr}}{S_{l\_SOI}\sigma} \tag{10}$$

where $\sigma = \rho_u/\rho_b$ is the ratio of unburned and burned products densities at SOI. The denominator corresponds to the speed of the flame front dR/dt under constant pressure assumption.

To normalize this characteristic time for the different engine speeds, the time (τ_t) taken by an eddy of the integral length scale size L to rotate at SOI is used:

$$\frac{\tau_{tr}}{\tau_t} = \frac{\frac{R_{tr}}{S_{l\_SOI}\sigma}}{\frac{L}{u'}} \tag{11}$$

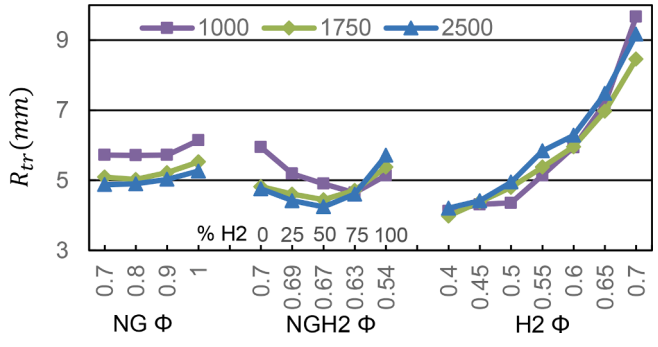

Fig. 4. Mean transition flame front radius R_{tr} for each test point. 1000, 1750 and 2500 rpm.

where u' is the turbulence intensity and L the turbulence integral length scale considered as the distance from the engine head to the piston in the spark plug position. All the variables except R_{tr}, are instantaneous variables calculated at SOI.

In this work, the mean turbulence intensity u' is calculated as by Giménez et al. [26], with a turbulence model for an open chamber gas engine [33]. The model has been used in AVL BOOST 1D software under motored engine conditions to simulate the flow during intake and closed valve cycle.

In Fig. 5 this relationship of times is shown for all test points. It is observed that the two times are comparable in magnitude.

This time ratio increases with the engine speed due to: the denominator variables of the characteristic transition time τ_{tr} do not depend on the engine speed; and R_{tr} depends very little, as can be seen in Fig. 4. However, the turbulence characteristic time decreases with the engine speed.

In NG and H2 the laminar combustion speed increases with fuel–air equivalence ratio and with H2 percentage. Therefore, the time relationship has a decreasing trend when the laminar combustion speed grows.

These two dependencies of time relationship on the turbulence and the laminar combustion speed are similar to the relationship between the turbulent combustion speed and the laminar combustion speed (flame speed ratio FSR) in any combustion process, as can be seen in the review of O.L. Gulder [34].

$$FSR = \frac{S_t}{S_l} = K\left(\frac{u'}{S_l}\right)^a \tag{12}$$

where K and a are always positive.

Fig. 6 shows the relationship between the turbulent combustion speed in R_{d_ini} and the laminar combustion speed at SOI S_{d_ini}/S_{l_SOI}. In short, the value by which the laminar combustion speed will be multiplied during the flame kernel growth. This value is very close to the

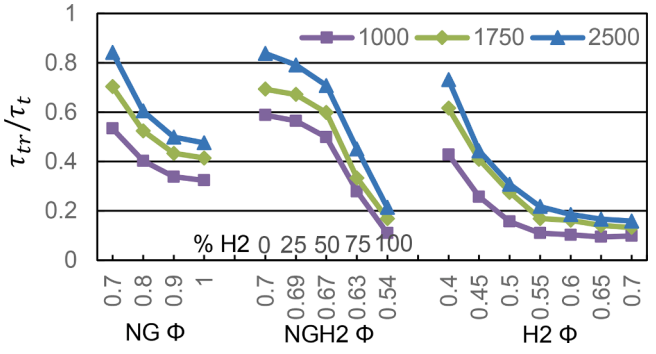

Fig. 5. Relationship of transition and turbulence mean characteristic times τ_{tr}/τ_t for each test point. 1000, 1750 and 2500 rpm.

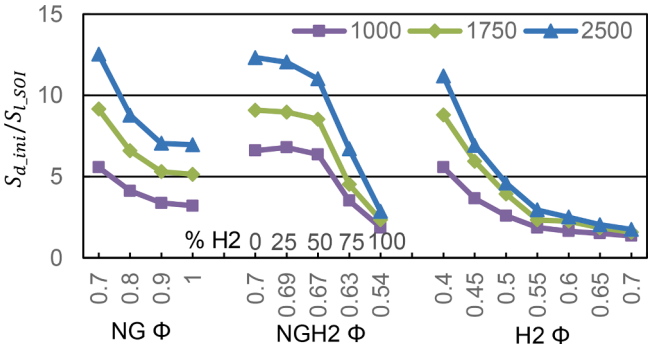

Fig. 6. Mean S_{d_ini}/S_{l_SOI} of each test point. 1000, 1750 and 2500 rpm.

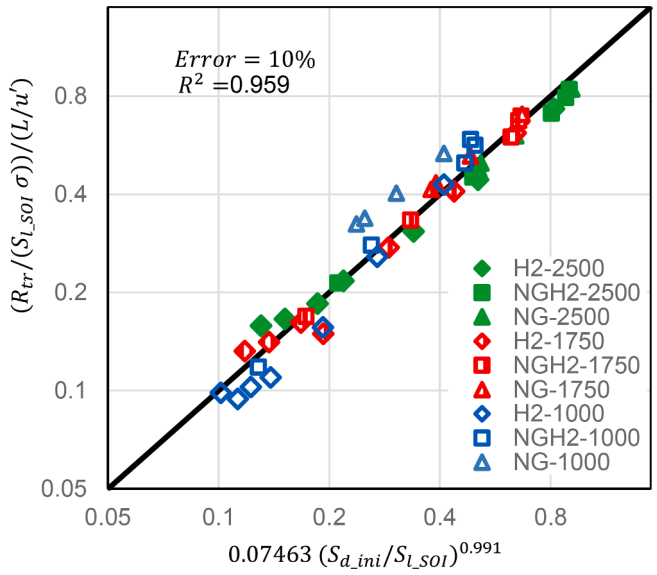

Fig. 7. τ_{tr}/τ_t value calculated from the mean values of each test versus the result of the correlation obtained with the exponential fit, for all test points.

conventional $FSR = S_t/S_l$ corresponding to the combustion speed ratio at a specific instant, since the laminar combustion speed barely varies during the flame kernel growth (Fig. 1). As expected, the trends predicted by the FSR correlations in Eq. (12) are fulfilled (decrease with laminar combustion speed and increase with turbulence intensity). A remarkable resemblance is observed in the trends of the characteristic times ratio and S_{d_ini}/S_{l_SOI}.

4.2. Correlations for the transition flame radium R_{tr}

4.2.1. Correlation with FSR

With the results obtained from all the experimental data, an exponential fit for the time ratio τ_{tr}/τ_t and S_{d_ini}/S_{l_SOI} has been performed. The latter can be considered as the ratio of times the flame front takes in traveling a distance at laminar and turbulent combustion speeds. In the fit, the exponent of S_{d_ini}/S_{l_SOI} is very close to unity. Fig. 7 shows the results of the adjustment for all engine speeds, mixtures and fuel–air

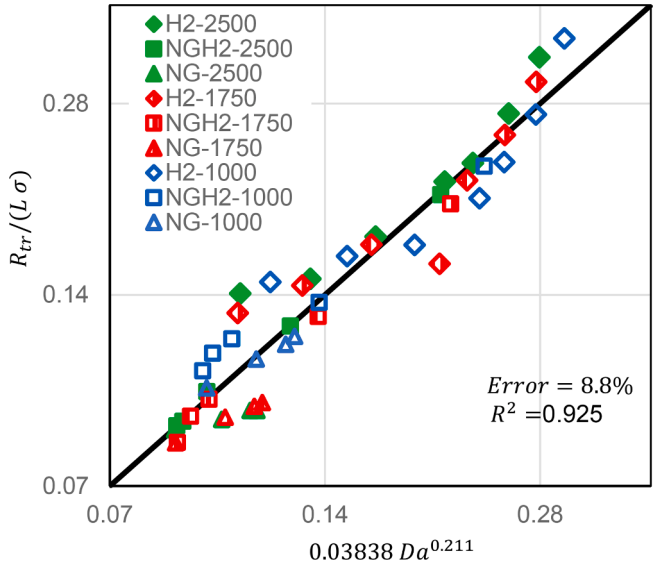

Fig. 8. $R_{tr}/(L\sigma)$ value calculated from the mean values of each test versus the result of the correlation obtained with the exponential fit to Damköhler number, for all test points.

equivalence ratios. The average relative error is 10 %.

The two times ratio can be correlated according to Eq. (13).

$$\frac{\frac{R_{tr}}{S_{l\_SOI}\sigma}}{\frac{L}{u'}} = K\frac{S_{d\_ini}}{S_{l\_SOI}} \tag{13}$$

Rearranging Eq. (13):

$$\frac{R_{tr}}{S_{d\_ini}\sigma} = K\frac{L}{u'} \tag{14}$$

The left term expresses a relationship between R_{tr} and the flame front speed after the transition, this relation only depends on the turbulence characteristics. In other words, for the same level of turbulence, the greater the turbulent combustion speed that will be reached after the transition, the greater is R_{tr}. Any combination of S_l (properties of the mixture) and FSR (properties of the fluid field) which the product takes the same value has the same consequences.

4.2.2. Correlation with Damköhler number.

On the other hand, Eq. (14) has a limited predictive character since it depends on the turbulent combustion speed S_{d_ini} in R_{d_min}. This combustion speed can be estimated based on the laminar combustion speed and the characteristic parameters of the turbulence. Turbulent combustion speed can be replaced by expressions like the ones in [35,36]:

$$S_{d\_ini} = Au'Da^b \tag{15}$$

The resulting expression is:

$$\frac{R_{tr}}{L\sigma} = KDa^b \tag{16}$$

Fig. 8 shows the adjustment of the experimental data using the variables $R_{tr}/(L\sigma)$ and Da.

The fitting result is:

$$\frac{R_{tr}}{L} = 0.0384\sigma Da^{0.21} \tag{17}$$

The value of $b = 0.21$ is consistent with the proposed in literature to predict turbulent combustion speed values [35,37,38] (b around 0.25).

The transition flame front radius and the integral length scale ratio depends on the product $\sigma Da^{0.21}$. Fig. 9 shows $Da^{0.21}$ and σ normalized with the average value of the test series (tests of NG, NGH2 and H2). It is observed that the trend of σ in the mixtures is the opposite to the Damköhler number. In the range of variation of the equivalence fuel air ratio, the influence of $Da^{0.21}$ is much greater than σ in H2 while in NG the influence of both is comparable.

If the Eq. (17) is expressed as a function of the magnitudes of the turbulence and the mixture properties:

$$R_{tr} = 0.0384\sigma L^{1.21}u' - 0.21S_l^{0.42}\alpha^{-0.21} \tag{18}$$

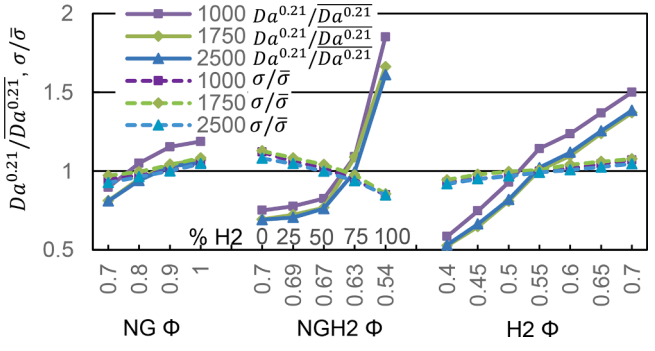

Fig. 9. $Da^{0.21}$ and σ normalized with the average value of each of the three test series (NG, NGH2 and H2).

Eq. (18) indicates that for a given fuel mixture, to reduce the mixture mass that burns in laminar regime (that is to reduce R_{tr}), the integral scale must be reduced (which has a more than linear effect) and the turbulence intensity must be increased (although this has a rather less than linear effect).

On the other hand, for fixed turbulence levels, the higher the density ratio, the higher the position at which the process changes from laminar to turbulent R_{tr}. This seems reasonable since the increase in σ implies an increase in expansion velocity and therefore an increase in the distance that the flame front travels (with the rest of conditions constant). Finally, the increase in the laminar combustion speed increases the distance in which the transition from laminar to turbulent regime occurs.

5. Conclusions

In our previous work [26] a correlation of the combustion speed was obtained for all tested operating conditions, valid during the whole combustion process except for the beginning. This work completes the previous one since now, combustion speed at the beginning can be predicted using the mixture properties in the combustion chamber. Therefore, the results are applicable for use with predictive models to calculate the pressure in the combustion chamber and consequently the engine performance.

The need to characterize the transition process from laminar to turbulent combustion that takes place in the first moments of combustion in SIE is clear. In this work a study has been carried out in order to develop a correlation that allows predicting when (for what radius of the flame front) the transition in the combustion speed occurs. The correlation depends on the characteristic parameters of the process. For this, data processing techniques that were developed in previous works have been used. In addition, a predictive model of flame kernel growth in the first stages of combustion has been developed.

The most detailed way to model this problem is by using CFD techniques based on chemical kinetics models to predict reaction rates, these techniques require a cell size smaller than the flame front thickness. In order to model the interaction of the eddies with the reaction zones it is also necessary to have a very small cell size. The computational cost of this methodology complicates its use in large test series with multiple operating points oriented to the development of new engines with new fuels. The methodology proposed in this work is based on using correlations of laminar combustion speeds for the modeling of chemical kinetics. For calculating the interaction with the fluid field, a correlation based on the Damköhler number is used. This alternative is several orders of magnitude faster in the estimation of the flame kernel growth duration for its use in the development of modern engines based on new fuels.

The adjustment of the predictive model to the burned mass experimental data for a certain position of the flame front allows to have a cycle-by-cycle estimation of the position of the flame front R_{tr} in which the transition in the combustion speed occurs. Once 500 cycles have been processed for each operating point, the mean values of R_{tr} have been related to the characteristic variables of turbulence and thermochemical processes that take place during combustion.

Using an approach based on two concepts put forward in various theoretical and experimental works: transition from laminar to turbulent and the position at which this occurs, a method has been developed to characterize the first phase of combustion with a single spatial parameter R_{tr}, while an angular or temporal parameter is commonly used in the bibliography.

From the analysis of this parameter, the following conclusions can be drawn:

- In general, and for the same fuel, the higher the laminar combustion speed at SOI, the greater the flame front radius for which combustion changes from laminar to turbulent.
- The integral length scale size is the most influential parameter in the value of R_{tr}. In order to reduce R_{tr}, and consequently the time in which the process is laminar, the piston-engine head distance near to the spark plug position, must be as small as possible.
- The value of R_{tr} is linearly proportional to the density ratio σ. The flame front speed is the product of σ and the combustion speed, therefore, if time is constant, the distance R_{tr} increases proportionally with σ. This can be interpreted as the phenomenology of the process is independent of σ, which acts as a geometric multiplier in the process.
- The characteristic time that the combustion speed takes to be turbulent has a lineal dependence with the eddies rotation time and the multiplicative effect that turbulence has on the combustion speed (FSR). This explains the fact that hydrogen has high transition front radii and small transition times due to its low FSR.
- For a given turbulence level L/u', the value of R_{tr} is proportional to the turbulent combustion speed that will exist after the transition.
- The characteristic time of transition is in the same order of magnitude as the rotation time of an integral length scale eddy.
- To improve the predictive nature of the correlation, the ratio R_{tr}/L can be expressed as a function of the density ratio and the Damköhler number. In the range of fuel–air equivalence ratios tested, the Damköhler number has a higher influence in H2 R_{tr} value than in NG R_{tr} value.

The results obtained are in agreement with the idea that the transition occurs when the flame front reaches the extremes of the integral length scale vortices and until that moment the flame front propagates with a speed close to laminar.

A novel pressure records processing based on careful data filtering allows to analyse the duration of the first phase of combustion and to extrapolate the combustion analysis to a spatial approach utilizing hypotheses used by other researchers.

Although a wide engine operating range has been used in the definition of the test plan, the maximum load and engine speed levels do not cover all possible operating ranges of SIE. This study can be extended to other fuels, combustion chamber geometries, engine speeds and loads. In this case, it should be considered that decreasing the laminar combustion speed, increasing the turbulence or decreasing the integral scale can move the test points to the thin reactions zone in the Borghi-Peters diagram.

CRediT authorship contribution statement

Blanca Giménez: Project administration, Writing – original draft, Resources, Conceptualization. **Andrés Melgar:** Methodology, Software, Formal analysis, Investigation. **Alfonso Horrillo:** Writing – review & editing, Supervision. **Pedro Gabana:** Visualization, Resources, Investigation.

Declaration of Competing Interest

The authors declare that they have no known competing financial interests or personal relationships that could have appeared to influence the work reported in this paper.

Data availability

Data will be made available on request.

Acknowledgments

Much of the research work carried out has been financed with funds from the Spanish government through the project “Analysis and characterization of dual fuel combustion for the reduction of CO_2 emissions in the transport sector” (PID2019-106957RB-C22).

P. Gabana has been funded by the 2021 call for predoctoral contracts from the University of Valladolid, co-financed by Banco Santander.

The authors would like to thank AVL Advanced Simulation Technologies for allowing the use of the AVL BOOST program in carrying out this work.

Mendeley Data

Giménez, Blanca; Melgar, Andrés; Horrillo, Alfonso; Tinaut, Francisco (2019), "Combustion speed in ICE: thermodynamic model for combustion speed, expansion speed, data base", Mendeley Data, v1. Published: 31 Jul 2019. DOI: 10.17632/wskmmkg6rk.1.

References

[1] Ayala FA, Heywood JB, Lean SI Engines: The role of combustion variability in defining lean limits, SAE Technical Paper Series 2007-24-0030. (2007). https://doi.org/10.4271/2007-24-0030.
[2] Wang Z, Su X, Wang X, Jia D, Wang D, Li J. Impact of ignition energy on the combustion performance of an SI heavy-duty stoichiometric operation natural gas engine. Fuel 2022;313:122857.
[3] Herweg R, Maly RR. A fundamental model for flame kernel formation in S. I engines. SAE Technical Paper Series 1992;922243. https://doi.org/10.4271/922243.
[4] Ozdor N, Dulger M, Sher E. Cyclic variability in spark ignition engines A literature survey. SAE Technical Paper Series 1994;940987. https://doi.org/10.4271/940987.
[5] Bradley D, Lawes M, Liu K, Verhelst S, Woolley R. Laminar burning velocities of lean hydrogen-air mixtures at pressures up to 1.0 MPa. Combust Flame 2007;149:162–72. https://doi.org/10.1016/j.combustflame.2006.12.002.
[6] Kumar P, Anil Kishan P, Nikhil Mathew M, Dhar A. Flame kernel growth study of spark ignited hydrogen air premixed combustion at engine conditions. Therm Sci Eng Progr 2021;21:100769. https://doi.org/10.1016/j.tsep.2020.100769.
[7] Nguyen MT, Shy SS, Chen YR, Lin BL, Huang SY, Liu CC. Conventional spark versus nanosecond repetitively pulsed discharge for a turbulence facilitated ignition phenomenon. Proc Combust Inst 2021;38(2):2801–8.
[8] Willems H, Sierens R. Modeling the initial growth of the plasma and flame kernel in SI engines. J Eng Gas Turbine Power 2003;125:479–84. https://doi.org/10.1115/1.1501912.
[9] Badawy T, Bao XC, Xu H. Impact of spark plug gap on flame kernel propagation and engine performance. Appl Energy 2017;191:311–27. https://doi.org/10.1016/j.apenergy.2017.01.059.
[10] Eisazadeh-Far K, Parsinejad F, Metghalchi H, Keck JC. On flame kernel formation and propagation in premixed gases. Combust Flame 2010;157:2211–21. https://doi.org/10.1016/j.combustflame.2010.07.016.
[11] Maly R. Ignition model for spark discharges and the early phase of flame front growth. Symp (Int) Combust 1981;18:1747–54. https://doi.org/10.1016/S0082-0784(81)80179-8.
[12] Lim MT, Anderson RW, Arpaci VS. Prediction of spark kernel development in constant volume combustion. Combust Flame 1987;69:303–16. https://doi.org/10.1016/0010-2180(87)90123-4.
[13] Pischinger S, Heywood JB. A model for flame kernel development in a spark-ignition engine. Symp (Int) Combust 1991;23:1033–40. https://doi.org/10.1016/S0082-0784(06)80361-9.
[14] Gatowski JA, Heywood JB, Deleplace C. Flame photographs in a spark-ignition engine. Combust Flame 1984;56:71–81. https://doi.org/10.1016/0010-2180(84)90006-3.
[15] Peterson B, Baum E, Böhm B, Dreizler A. Early flame propagation in a spark-ignition engine measured with quasi 4D-diagnostics. Proc Combust Inst 2015;35(3):3829–37.
[16] Schiffmann P, Reuss DL, Sick V. Empirical investigation of spark-ignited flame-initiation cycle-to-cycle variability in a homogeneous charge reciprocating engine. Int J Engine Res 2018;19:491–508. https://doi.org/10.1177/1468087417720558.
[17] Zeng W, Keum S, Kuo T-W, Sick V. Role of large scale flow features on cycle-to-cycle variations of spark-ignited flame-initiation and its transition to turbulent combustion. Proc Combust Inst 2019;37(4):4945–53.
[18] Yaşar O. New ignition model for spark-ignited engine simulations. Parallel Comput 2001;27:179–200. https://doi.org/10.1016/S0167-8191(00)00094-6.
[19] Colin O, Truffin K. A spark ignition model for large eddy simulation based on an FSD transport equation (ISSIM-LES). Proc Combust Inst 2011;33(2):3097–104.
[20] Wadekar S, Janas P, Oevermann M. Large-eddy simulation study of combustion cyclic variation in a lean-burn spark ignition engine. Appl Energy 2019;255:113812.
[21] Su Y, Splitter D, Kim SH. Laminar-to-turbulent flame transition and cycle-to-cycle variations in large eddy simulation of spark-ignition engines. Int J Engine Res 2021;22:2803–18. https://doi.org/10.1177/1468087420962346.
[22] Keum S, Zhu G, Grover R, Zeng W, Rutland C, Kuo T-W. A semi-empirical laminar-to-turbulent flame transition model coupled with G equation for early flame kernel development and combustion in spark-ignition engines. Int J Engine Res 2021;22(2):479–90.
[23] d'Adamo A, Iacovano C, Fontanesi S. Large-Eddy simulation of lean and ultra-lean combustion using advanced ignition modelling in a transparent combustion chamber engine. Appl Energy 2020;280:115949. https://doi.org/10.1016/j.apenergy.2020.115949.
[24] Pera C, Knop V, Reveillon J. Influence of flow and ignition fluctuations on cycle-to-cycle variations in early flame kernel growth. Proc Combust Inst 2015;35(3):2897–905.
[25] Salvi BL, Subramanian KA. Experimental investigation and phenomenological model development of flame kernel growth rate in a gasoline fuelled spark ignition engine. Appl Energy 2015;139:93–103. https://doi.org/10.1016/j.apenergy.2014.11.012.
[26] Giménez B, Melgar A, Horrillo A, Tinaut FV. A correlation for turbulent combustion speed accounting for instabilities and expansion speed in a hydrogen-natural gas spark ignition engine. Combust Flame 2021;223:15–27. https://doi.org/10.1016/j.combustflame.2020.09.026.
[27] Savitzky A, Golay MJE. Smoothing and differentiation of data by simplified least squares procedures. Anal Chem 1964;36(8):1627–39.
[28] Reyes M, Melgar A, Pérez A, Giménez B. Study of the cycle-to-cycle variations of an internal combustion engine fuelled with natural gas/hydrogen blends from the diagnosis of combustion pressure. Int J Hydrogen Energy 2013;38:15477–87. https://doi.org/10.1016/j.ijhydene.2013.09.071.
[29] Giménez B, Melgar A, Horrillo A, Tinaut F. Combustion speed in ICE: thermodynamic model for combustion speed, expansion speed, data base. Mendeley Data 2019;V1. https://doi.org/10.17632/wskmmkg6rk.1.
[30] Bougrine S, Richard S, Nicolle A, Veynante D. Numerical study of laminar flame properties of diluted methane-hydrogen-air flames at high pressure and temperature using detailed chemistry. Int J Hydrogen Energy 2011;36:12035–47. https://doi.org/10.1016/j.ijhydene.2011.06.053.
[31] Borghi R. Turbulent combustion modelling. Prog Energy Combust Sci 1988;14:245–92. https://doi.org/10.1016/0360-1285(88)90015-9.
[32] Peters N. The turbulent burning velocity for large-scale and small-scale turbulence. J Fluid Mech 1999;384:107–32. https://doi.org/10.1017/S0022112098004212.
[33] Schlick H, Pirker G, Chmela F, Wimmer A, Weiterentwicklung eines nulldimensionalen brennratenmodells für direktgezündete gasmotoren auf basis der computertomographie (improving the predictive capability of a zerodimensional combustion model for open-chamber gas-engines based on computer tomography), Engine Combust Process Curr Probl Mod Tech. 2009;115–126.
[34] Gulder OL. Turbulent premixed flame propagation models for different combustion regimes. Symp (Int) Combust 1990;23:743–50. https://doi.org/10.1016/S0082-0784(06)80325-5.
[35] Zimont VL. Gas premixed combustion at high turbulence. Turbulent fame closure combustion model. Exp Therm Fluid Sci 2000;21:179–86. http://hdl.handle.net/11050/1040.
[36] Karpov VP, Severin ES. Effects of molecular-transport coefficients on the rate of turbulent combustion. Combust Explos Shock Waves 1980;16:41–6. https://doi.org/10.1007/BF00756242.
[37] Lipatnikov AN, Chomiak J. Turbulent Fame speed and thickness: phenomenology, evaluation, and application in multi-dimensional simulations. Prog Energy Combust Sci 2002;28:1–74. https://doi.org/10.1016/S0360-1285%2801%2900007-7.
[38] Liu K, Burluka AA, Sheppard CGW. Turbulent flame and mass burning rate in a spark ignition engine. Fuel 2013;107:202–8. https://doi.org/10.1016/j.fuel.2013.01.042.